The Expansion of Colloid Thruster Beams

IEPC-2009-175

Presented at the 31st International Electric Propulsion Conference,
University of Michigan • Ann Arbor, Michigan • USA
September 20 – 24, 2009

M. Gamero-Castaño [1]
University of California, Irvine, California, 92697, USA

Abstract: Colloid thrusters are electrostatic accelerators of charged droplets and ions generated by electrosprays. The low thrust and high thrust stability associated with a single emitter are ideal for precision spacecraft positioning applications. This technology will be tested in the Disturbance Reduction System-Space Technology 7 mission, which is a precursor of the Laser Interferometer Space Antenna mission. Although the colloid thruster engine for DRS/ST7 is fully developed and demonstrated, the structure of the electrospray beams are relatively unknown. A good understanding of the beam is necessary to assess its interaction with spacecraft surfaces, and to design optimally the accelerating electrodes of the thruster. This article presents a model for resolving the structure of the beams of EMIIm, the propellant employed by the ST7 thruster. These electrosprays are formed by populations of charged droplets and molecular ions. We use an Eulerian formulation to compute the trajectories of beam particles, and replicate the space charge with a model of charged droplets distributed along the axis of the beam. A detailed experimental characterization of the EMIIm beams provides insights and input parameters for the model, and ultimately validates the calculations.

I. Nomenclature

D	=	droplet diameter
I_B	=	beam current
q_R	=	Rayleigh limit, maximum charge that can be held by a stable droplet
R	=	radial position of a droplet trajectory
v	=	axial component of the droplet velocity vector
v_j	=	jet velocity at breakup
z	=	axial coordinate
ε_0	=	vacuum permittivity
γ	=	surface tension
λ	=	average wavelength of the jet breakup
ξ	=	charge to mass ratio
ϕ_E	=	emitter potential
ρ	=	liquid density

[1] Assistant Professor, Department of Mechanical and Aerospace Engineering, mgameroc@uci.edu

II. Introduction

DETECTION of gravitational waves in space via projects such as LISA and a variety of projected future missions involving formation flying of multiple spacecrafts, require exquisitely fine thrust control at the microNewton level. In addition, the capability for occasionally yielding higher thrust would be a plus. Colloid thrusters may be the only technology that can provide both requirements simultaneously. Colloid thrusters will be demonstrated on NASA's ST7. Nevertheless, this technology is still in its infancy, and different thruster related phenomena are poorly understood and/or remain to be investigated. The spreading of the colloid thruster beam is one of such phenomena. Knowledge on how the electrospray beam behaves, and the ability to manipulate it, can be used to improve two performance parameters of the colloid thruster: first, spacecraft contamination could be eliminated by reducing beam spreading; second, a larger beam current, and hence thrust, can be passed through the extracting electrodes if the beam spreading is reduced. The latter could increase considerably the throttling range of the colloid thruster, which would now have the potential to be used for cancellation of initial spacecraft tip-offs and safe mode actions, in addition to its nominal drag cancellation function.

The spreading of the beam is determined by two processes: initially, electrostatic forces induced by the beam's space charge opens up the beam. This happens within a small region downstream of the emitter. After this initial dominance, the space charge field becomes negligible compared to that induced by the distribution of charge on the emitter and extractor electrodes. This article aims at obtaining a first-principles understanding of the structure of the electrosprays of EMIIm, the propellant of the ST7 colloid thrusters.[1] To that end, we formulate an Eulerian model to compute the trajectories of beam particles. An essential part of the model is our treatment of the beam's space charge, which is replicated with a distribution of charges along the axis of the beam. A detailed experimental characterization of the EMIIm beams provides insights and input parameters for the model, and ultimately validates its results. We use a simple emitter-extractor diode configuration throughout this study.

III. Beam Structure

Our beam model divides the distribution of beam particles into groups of particle having identical diameter, charge to mass ratio and initial velocities, and computes the axisymmetric envelop surrounding each group. Groups of particles interact with each other through an electric force (space charge), which appears explicitly in the equation of motion of the droplets defining each envelop. The required particle distribution, initial conditions for the trajectories, and electric potential at the emission point are measured via time of flight and retarding potential techniques.[2] The experimental characterization also measures the structure of the beam, which is later used for a positive comparison with the model results.

A. Experimental Characterization

Figure 1 shows a sketch of the experimental setup.[3] The electrospray source, placed inside a vacuum chamber, atomizes the EMIIm propellant stored in an external tank. The flow rate of propellant is controlled by modifying the pressure in the tank. A high voltage power supply electrifies the emitter; the potential of the emitter is typically 1700 V. A shunt resistor is used to monitor the beam current. The beam of charged droplets and molecular ions produced by the electrospray source is analyzed with a cumulative retarding potential analyzer (RPA) with a sampling orifice of 4.97 mm^2; a fast electrometer with an identical sampling area of 4.97 mm^2; and a second fast electrometer connected to a larger collector. The electrometers measure the time of flight waves associated with either a small area of the beam, or the whole beam respectively. Time of flight waves are generated by suddenly shorting the emitter potential to ground with a high voltage switch, which interrupts the

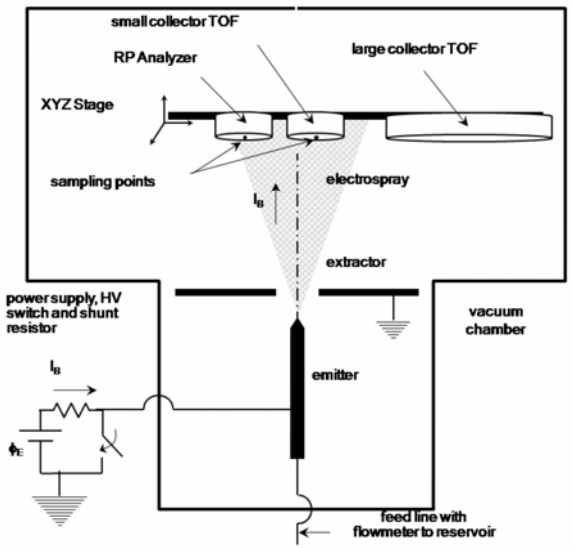

Figure 1. Experimental setup used to characterize electrospray beams in vacuum.

fluid atomization. The detectors are mounted on an XYZ positioning stage to sample the beam at different locations. The retarding potential and time of flight data captured with the 4.97 mm^2 detectors yield the charge to mass ratio distribution of the beam as a function of position. The electrometer inside the cumulative RPA is also used to measure current density as a function of position, i.e. to measure beam profiles. Finally, the large collector is used to measure the velocity distribution of the whole beam. The beam mass flow rate is computed from the integration of this global measurement.[4]

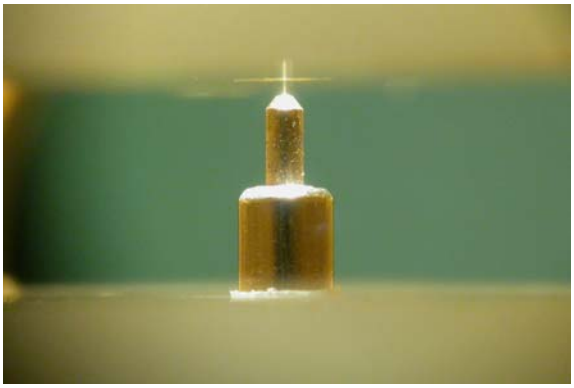

Figure 2. Emitter-extractor geometry.

Figure 2 shows the emitter and extractor geometry of the electrospray source. The emitter is a platinum tube with a 0.480 mm outer diameter, and a 0.160 mm inner diameter. The tip is chamfered at a 42 deg angle. In the calculation of the electrostatic field we assume that the Taylor cone anchored on the base of the tip has the same angle of the chamfer. The extractor plane is 0.076 mm downstream from the vertex of the Taylor cone, it has an orifice with a diameter of 1.2 mm, and a thickness of 0.5 mm.

Figures 3 to 6 display the basic characteristics of these beams. Figure 3 shows beam profiles as a function of beam current. The beam is sampled in a plane perpendicular to the beam axis, 12 cm downstream from the electrospray source emission point. Note that the beam is relatively narrow at the lowest beam currents, and broadens up as the current increases. The beams are slightly asymmetric, most likely because of geometrical asymmetries in the electrospray source. After averaging both sides of each profile, we compute the angle of conical envelopes that contain a given fraction of the beam current. These curves are shown in Fig. 4. The angle of the beam associated with a given beam current fraction is roughly proportional to the total beam current. Figures 5 and 6 show retarding potential and time of flight distributions as a function of separation from the beam axis (radial distance in cylindrical coordinates), for a beam current of 540 nA. Both ions and droplets are observed near the beam axis, but the ion population disappears near the beam edge. The location of the sampling points is shown in Fig. 3 in the form of symbols on the profiles. The absence of ions in the outer region of the beam occurs for all beam currents within the studied range, 216 nA – 850 nA. This observation is paradoxical according to what we know from the modeling and measurement of beams of propylene carbonate electrosprayed droplets.[2] The smaller droplets in these beams (referred to as satellite droplets), which like EMIIm ions have the largest charge to mass ratios in the beam, segregate from larger and less charged droplets (referred to as main droplets), and form an outer beam surrounding

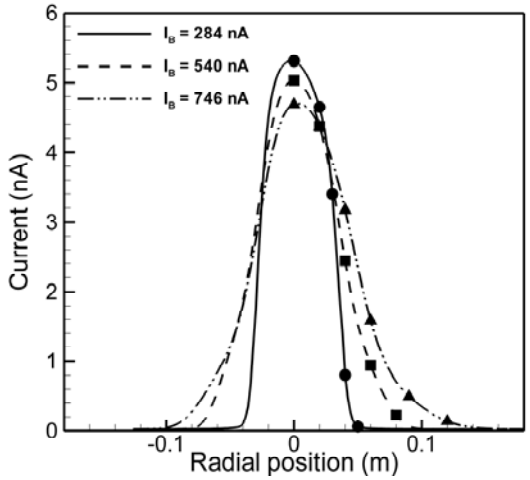

Figure 3. Beam profiles for three beam currents.

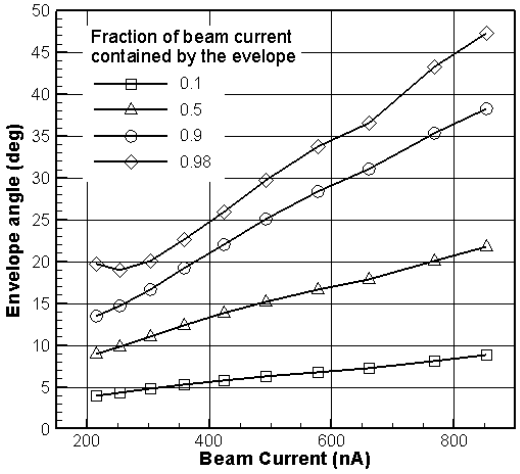

Figure 4. Angle of the envelope containing a given fraction of the beam current, for beam currents in the 216 nA – 850 nA range.

the inner beam of main droplets. We had expected that the ions present in EMIIm beams would form an outer beam similar to that of propylene carbonate satellite droplets.

The beam model requires an estimate of the diameter of EMIIm droplets. It is known that the charge of larger electrosprayed droplets is typically between 1 and 0.5 the Rayleigh stability limit, or maximum charge that a droplet can have without undergoing a Coulombic explosion.[5] These limits place upper and lower bounds on the diameter

$$\left(72\gamma\varepsilon_0/\rho^2\xi^2\right)^{1/3} < D < \left(288\gamma\varepsilon_0/\rho^2\xi^2\right)^{1/3} \quad (1)$$

The 50% limit is an approximation that has been demonstrated for micron-sized electrospray droplets,[6] as well as for EMIIm nanodroplets.[7] The average ratio between the charge of an EMIIm droplet and its Rayleigh limit approximately is $\langle q/q_R \rangle = 0.679$,[7] and we will use this value to estimate the average diameter of a EMIIm droplet with known charge to mass ratio.

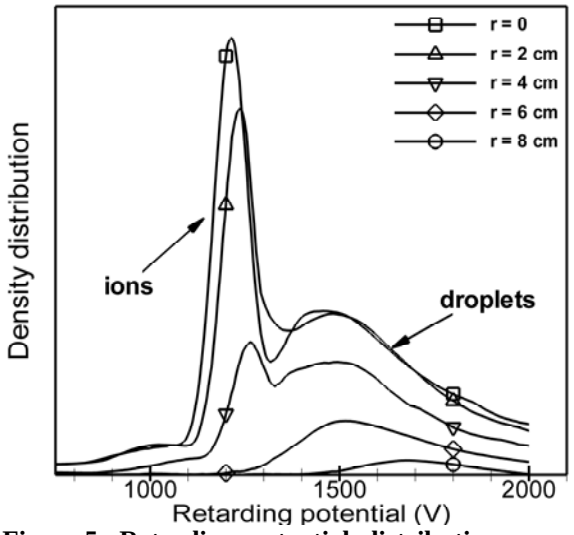

Figure 5. Retarding potential distributions as a function of radial position from the beam axis, for I_B = 540 nA.

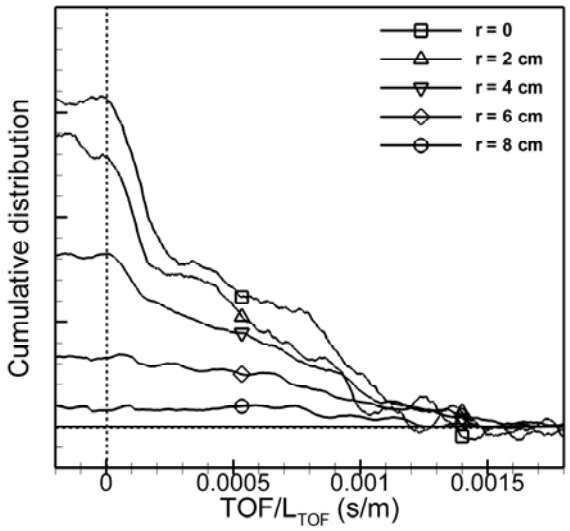

Figure 6. Time of flight distributions as a function of radial position from the beam axis, for I_B = 540 nA..

B. Beam Model

We have previously modeled the beams of electrosprayed droplets by first separating the droplets into beamlets of particles with equal properties, followed by the integration of the trajectory of a particle moving along the envelope surrounding the beamlet. The force acting on the trajectory is the electrical force induced by both the external electrodes, and the accumulated space charge of the beamlets. The latter term introduces a coupling between the beamlets. The equations of the model are:[2]

$$v_{ij}^2 \frac{d^2 R_{ij}}{dz^2} + v_{ij} \frac{dv_{ij}}{dz} \frac{dR_{ij}}{dz} = \frac{\xi_i \kappa_{ij} I_B \lambda}{2\pi\varepsilon_0 v_J} \left[\frac{8R_{ij}}{\left((\lambda+\lambda_i)^2 + 4R_{ij}^2\right)^{3/2}} + \frac{\sqrt{4R_{ij}^2 + (2\lambda+\lambda_i)^2} - (2\lambda+\lambda_i)}{R_{ij}\sqrt{4R_{ij}^2 + (2\lambda+\lambda_i)^2}} \right] + \xi_i E_r^{ext} \quad (2)$$

$$v_{ij} \frac{dv_{ij}}{dz} = \xi_i E_z^{ext} \quad (3)$$

$$\mathbf{E}^{ext} = -\nabla\phi^{ext} \quad (4)$$

$$\phi^{ext}(z_0) = \phi_J, R_{ij}(z_0) = \frac{j}{n} R_J, R'_{ij}(z_0) = 0, v_{ij}(z_0) = v_{0ij} \quad (5)$$

$$\kappa_{ij}(z) = \frac{\sum I_{kl}, \forall k,l \ni R_{kl}(z) \le R_{ij}(z)}{\sum I_{kl}, \forall k,l \ni R_{kl}(z) \le R_{in}(z)} \quad (6)$$

The first and second equations are the equations of motion for the beamlet trajectories, in terms of the radial position $R_{ij}(z)$ and axial velocity $v_{ij}(z)$ of a beamlet particle. The sub-indexes *ij* refer to a particular beamlet: the droplet population is first divided into $i = 1, \ldots, n$ groups having the same diameter and charge to mass ratio; a second division of each group into $j = 1, \ldots, m$ subgroups improves the resolution and assigns different initial velocities to the droplets. ξ_i is the charge to mass ratio of the particles. $\mathbf{E}^{ext}$ is the electric field induced by the external electrodes, which is computed with a numerical solver of the Laplace equation. The first term in the right hand side of (2) models the Coulombic interaction between beamlets, i.e. the forces associated with the beam's space charge. The equations in line (5) are the initial conditions for the trajectories and the value of the electric potential at the emission point. These parameters can be calculated from the time of flight and retarding potential measurements.[3] κ_{ij} in Eq. (2) is a numerical factor that quantifies the fraction of the beam current contained within the envelop *ij*, and is given by Equation (6).

This model reproduces well the expansion of electrospray beams with bimodal droplet populations (main and satellite droplets).[2] In the case of EMIIm beams, the population of molecular ions is a new feature that needs to be incorporated. Because the space charge induced by the ion beam is much smaller than that of the droplet beam (the similar beam broadness and much higher ion velocity result in an ion charge density significantly lower), we use the following simplification: first, we integrate the trajectories of droplets forced by the electric field induced by the electrodes and the space charge of the droplets only. After this initial step, the trajectories of ions are computed forced by the external electric field and the known space charge of the droplet beam.

C. Model Solution and Comparison with Experimental Results

Figure 7(a) shows several envelopes of droplet beamlets for a total beam current of 400 nA. We have divided the droplet population in 10x7 beamlets. The integration of the trajectories is stopped at z = 1 mm because the force acting on the droplets around and beyond this plane is negligible, and therefore the trajectories become straight lines. This is illustrated in Figure 7(b), where we plot the local angle of the trajectories. The constancy of the tangents of the trajectories makes it possible to use the computed angle at z = 1 mm to define the exit angle of the beamlets, which can in turn be compared with the experimental measurements. The exit angle for the broadest envelope (i.e. that including 100% of the beam current) is 26.8 deg. This angle compares well with the measured beam angle for I_B = 400 nA shown in Fig. 4. The current transported by beamlets with exit angles smaller than a given value α can be added to compute the current surrounded by an envelope of angle α. This value can then be compared with experimental measurements, as shown in Fig. 8. Note that the model and experimental results agree well. The

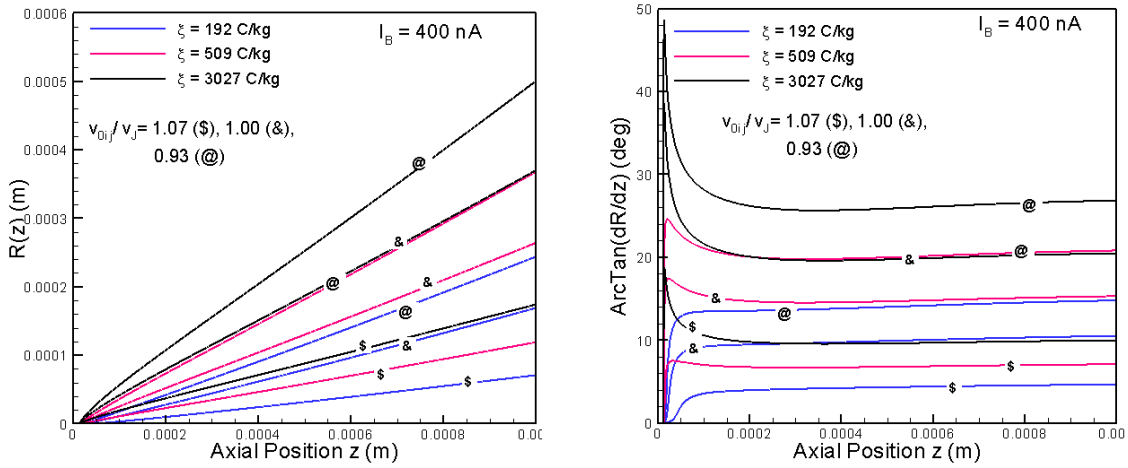

Figure 7.Trajectories and the local angle of the trajectories of several droplet beamlets, for a I_B = 400 nA.

experimental curve is steeper than the calculated, probably because the former includes the current associated with the ion population, which distributes preferentially in the inner region of the beam.

Figure 9 shows the beam angle (exit angle of the envelope containing 100% of the beam current) computed for beam currents in the rage 216 nA – 850 nA, together with the experimental values of Fig. 4. There is a good agreement throughout the current range. It is worth noting that the beam model does include free parameters that can be adjusted to improve the solution. Instead, all input parameters required by the model (distributions of droplet diameters, charge to mass ratios, and initial velocities; and electric potential at the emission point) are measured using time of flight and retarding potential techniques.

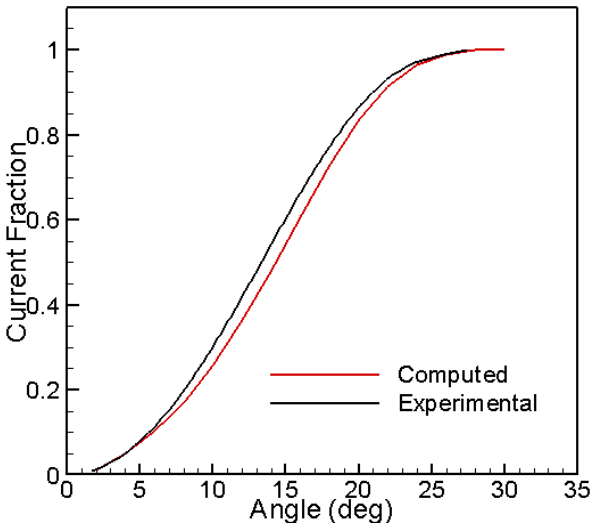

Figure 8. Fraction of the beam current under a given polar angle for I_B = 400 nA. The computed result only includes the current associated with droplets, while the experimental distribution includes both droplets and ions.

We can now integrate the equation of motion of ions emitted at or near the location of the jet breakup. We use the charge to mass ratio of EMI^+ and, since the ions are emitted from the surface of droplets, the velocity imparted by the electric potential of a typical droplet as its initial velocity. The electric field induced by the computed distribution of charged droplets, together with that induced by the external electrodes, acts on the ions. Figure 10 shows droplet (colored curves) and ion (black curves) trajectories for a 400 nA beam. λ refers to the average wavelength for the jet breakup, and which is used as a characteristic length to make the model equations non-dimensional. The initial axial position of ions and droplets are identical in this solution. It is not surprising that most ion trajectories surround the beam of droplets, because of the lower initial inertia of the ions, which makes them more sensitive to the diverging force of the space charge. More correctly, it is the factor v_0^2/ξ (i.e. the retarding potential of the charged particle), which for ions is smaller than for droplets, what makes the former more sensitive to the space charge field. There could be several sources for the disagreement between the calculated ion trajectories and the experimental observations. We do not think that the disagreement is the result of shortcomings of the space charge model, because the model of a line of point charges captures the relevant physics of the space charge in the initial region where its associated force dominates.[2] Furthermore, the results obtained with this model for beams of satellite and main droplets, as well as for EMIIm droplets, compare well with actual measurements. We think that the problem in Fig. 10 lies with an invalid initial position for the ions. In fact, the trajectories of ions are very sensitive to the axial location of their initial positions. This is shown in Fig. 11, where we start the integration of ion trajectories 60 λ units downstream from the droplet emission point. The length of the jet is 313 λ units (i.e. 12.5 μm), while the voltage difference between both emission points is only 30 V (the potential of the droplet emission point is 1316 V). In this case, all ion trajectories remain inside the droplet beam. Clearly, a considerable fraction of the droplet trajectories depart from the axis before they reach the ion emission point, and the space charge fields associated with these external beamlets do not exert a net radial force on the ions.

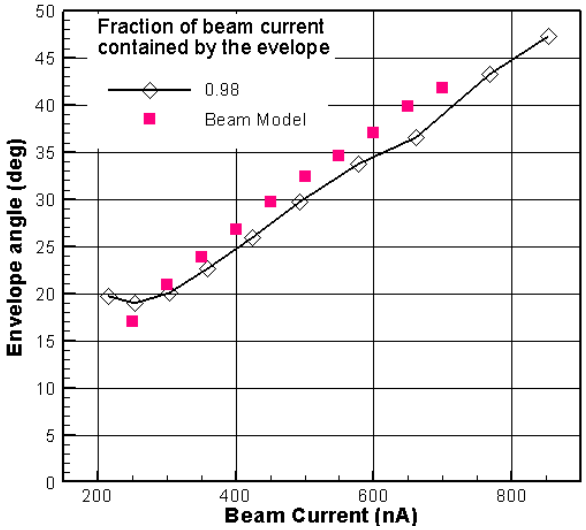

Figure 9. Computed and experimental beam angle as a function of beam current.

We think that the emission of ions from a downstream location makes physical sense. Ions are field emitted from the liquid surfaces with highest electric fields. From the comparison between experimental observations and model results, it is obvious that ion emission does not occur from the unbroken jet or jet filaments (i.e. upstream from the average breakup location), because in this case all ion trajectories would surround the droplet beam. Instead, ions

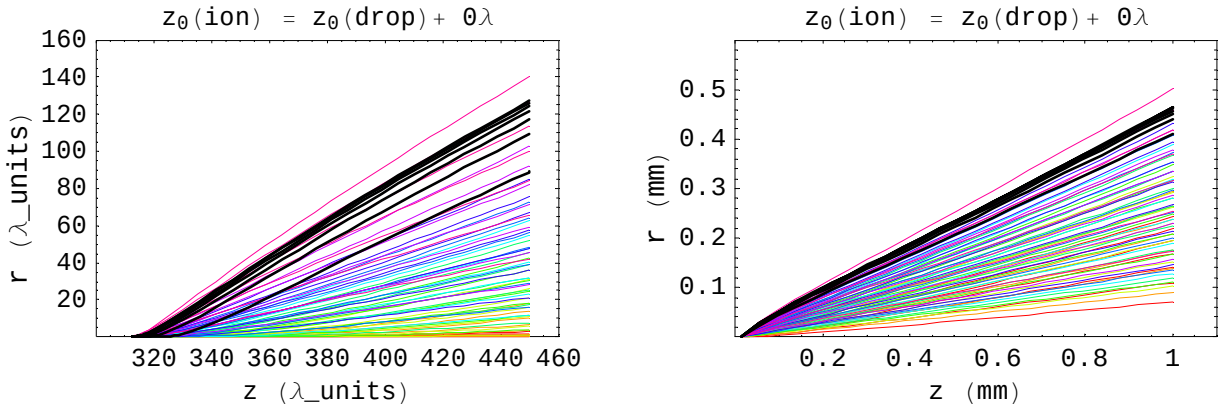

Figure 10. Droplet (colored) and ion (black) trajectories when the location of the emission points for droplets and ions are identical. The figure on the left offers a close-up view of the emission region.

must be emitted from a few droplets with the largest electric fields. We think that these few droplets are actually the largest droplets in the beam. The reason for this is that, for droplets with identical charge to mass ratios, the electric field on the surface increases is proportional to the droplet diameter. Furthermore, it is well known that the growth rate of an unstable disturbance is a function of the disturbance wavelength or, in other words, of the diameter of the droplet associated with the disturbance. The growth rate displays a maximum at a critical wavelength, and this

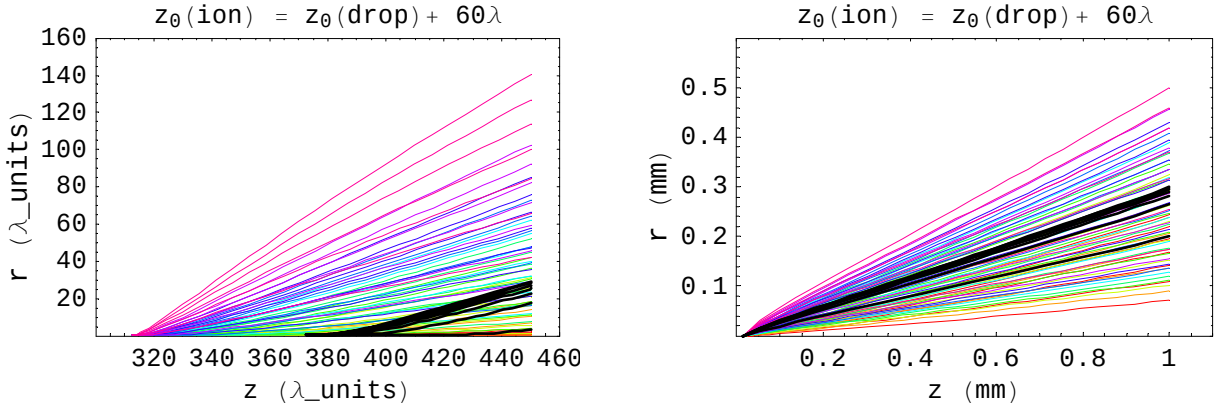

Figure 11. Droplet and ion trajectories when the ions are emitted slightly downstream of the droplet emission point.

critical wavelength yields the mean droplet diameter of the distribution. Droplets with diameters smaller or larger than the mean take a longer time to develop than the average droplets, and therefore would form farther downstream than the droplets with the average diameters (and fastest growth rates).

IV. Conclusion

The model of droplet envelopes reproduces well the structure of the beams of electrosprayed EMIIm, the ionic liquid propellant used for the ST7 mission. The accuracy of the model has been demonstrated by comparing the model results with experimental measurements associated with a simple emitter-extractor diode configuration. Since the main simplification of the model is its treatment of the space-charge dominated region near the electrospray emission point, which is independent of the electrode configuration, the same model can be used to study the beam expansion in any particular colloid thruster geometry, e.g. one having different emitter and extractor dimensions and/or additional electrodes, such as an accelerator plate. We plan to carry on with this research to study the optimization of the electrode configuration of an actual colloid thruster.

References

[1] J.K. Ziemer, T.M. Randolph, G.W. Franklin, V. Hruby, D. Spence, N. Demmons, T. Roy, E. Ehrbar, J. Zwahlen, R. Martin, W. Connolly, Delivery of flight qualified colloid micro-newton thrusters for the Space Technology 7 Mission, AIAA 2008-4826, 44th AIAA/ASME/SAE/ASEE Joint Propulsion Conference and Exhibit (2008).

[2] M. Gamero-Castaño, "The Structure of Electrospray Beams in Vacuum", Journal of Fluid Mechanics, 604, 339-368 (2008)

[3] M. Gamero-Castaño, "Characterization of the Electrosprays of 1-Ethyl-3-Methylimidazolium Bis(Trifluoromethylsulfonyl) Imide in Vacuum", Physics of Fluids 20, 032103 (2008). Also in The Virtual Journal of Nanoscale Science & Technology, Vol. 17, Issue 15 (2008).

[4] M. Gamero-Castaño & V. Hruby. "Electrospray as a source of nanoparticles for efficient colloid thrusters", Journal of Propulsion and Power, 17, 977-987 (2001).

[5] J. Fernández de la Mora, "On the outcome of the Coulomb fission of a charged isolated drop", Journal of Colloid and Interface Science, 178, 209 (1996).

[6] L. de Juan and J. Fernández de la Mora, "size and charge distributions of electrospray drops, J. Coll. and Interface Sci, 186, 280-293 (1997).

[7] M. Gamero-Castaño, "Retarding potential and induction charge detectors in tandem for measuring the charge and mass of nanodroplets", Review of Scientific Instruments, 80, 053301 (2009).